ELSEVIER

Contents lists available at ScienceDirect

Engineering Geology

journal homepage: www.elsevier.com/locate/enggeo





Feasibility of satellite-based rainfall and soil moisture data in determining the triggering conditions of debris flow: The Jiangjia Gully (China) case study

Hongjuan Yang, Kaiheng Hu*, Shaojie Zhang, Shuang Liu

Key Laboratory of Mountain Hazards and Earth Surface Process, Institute of Mountain Hazards and Environment, Chinese Academy of Sciences, Chengdu 610041, China

ARTICLE INFO

Keywords:
Debris flow
Rainfall threshold
Antecedent precipitation
Remote sensing

ABSTRACT

Heavy precipitation is the main trigger for debris-flow hazards. The antecedent moisture condition, which is usually represented by antecedent precipitation, is another hydrometeorological contributing factor to debris flows that originate from shallow landslides. Satellite techniques are an economical and effective way to access rainfall and soil wetness information to determine the triggering conditions of debris flow. However, satellitebased thresholds need to be compared with ground-based thresholds and adjusted to the data source prior to their application. In this study, rainfall intensity-duration (I-D) thresholds were derived from the early and final run products of the Integrated Multi-satellitE Retrievals for Global Precipitation Measurement (IMERG-E and IMERG-F) and gauge measurements using logistic regression for debris flows in the Jiangjia Gully, Yunnan Province, southern China, which has a dense rain gauge network. Data from both the IMERG-E and IMERG-F covered the entire study period. Our evaluation revealed that the I-D threshold derived from the IMERG-E deviated from the gauge-based thresholds. Although the threshold determined by the IMERG-F was comparable to the ground-based ones, the presence of substantial false positives and false negatives indicated that its performance was weaker than that of the gauge-based ones. Furthermore, the IMERG-F was suitable if the nearest available gauge was farther than 10 km from the debris-flow initiation zone. We evaluated the feasibility of the surface soil moisture product provided by the Climate Change Initiative program of the European Space Agency (CCI-SM), root-zone soil moisture derived from the CCI-SM using an exponential filter (SM-RZ), and antecedent precipitation for improving the performance of the thresholds by separately using them as the third explanatory variable in addition to rainfall intensity and duration in logistic regression. Satellite soil moisture data were available for 54% of the study period. The results suggested that including antecedent precipitation effectively improved the performance of the thresholds. In contrast, the performance of the thresholds increased only slightly when the CCI-SM or SM-RZ was included. Although these findings are valid only for this study area and need to be assessed for other regions, they present new insights for using satellite rainfall and soil moisture estimates to define thresholds for debris flow.

1. Introduction

Debris flows occur when masses of poorly sorted sediment that are agitated and saturated with water surge down slopes due to gravity (Iverson, 1997). Because of their high velocity and sediment volume, torrential debris-flow events endanger human lives and infrastructure. A catalogue compiled by Dowling and Santi (2014) reported 77,779 deaths from 213 global debris-flow events that occurred during 1950–2011. To mitigate debris-flow hazards, local or regional rainfall thresholds that indicate the triggering rainfall conditions of such

hazards have been proposed using historical data (Coe et al., 2008; Badoux et al., 2009; Staley et al., 2013; Zhuang et al., 2015; Giannecchini et al., 2016; Neptune et al., 2021).

Debris flows are initiated in two ways. They either originate from landslides (Iverson et al., 1997) or occur when the accumulated matter on hillslopes or in channels gets eroded and is mobilized by runoff (Gregoretti et al., 2016). Both physical simulations and in-situ measurements have highlighted the importance of antecedent soil moisture content in triggering shallow landslides as increased moisture content increases the soil weight and reduces matric suction (Tsai and Tsai and

^{*} Corresponding author at: Institute of Mountain Hazards and Environment, Chinese Academy of Sciences, Chengdu 610041, China. *E-mail address:* khhu@imde.ac.cn (K. Hu).

Chen, 2010; Hawke and McConchie, 2011; Mirus et al., 2018; Marino et al., 2020; Wicki et al., 2020). Therefore, it is expected that antecedent soil moisture conditions also impact triggering rainfall conditions of debris flows that originate from landslides (Johnson and Sitar, 1990). Existing studies have reported conflicting results on the importance of antecedent soil moisture in triggering runoff-generated debris flows. Some studies have shown that antecedent soil moisture is not significant in predicting debris-flow events (Deganutti et al., 2000; Coe et al., 2008; Hirschberg et al., 2021). However, a study from the Réal Torrent in the Southern French Prealps, showed that antecedent rainfall contributes to debris-flow triggering (Bel et al., 2017). Due to the lack of ground soil moisture observations, antecedent soil moisture is commonly substituted by antecedent precipitation in landslide forecasting models (Tien Bui et al., 2013; Vasu et al., 2014; Garcia-Urquia, 2016; Chikalamo et al., 2020; Ni and Song, 2020). In recent years, satellite soil moisture products have been used in landslide hazard assessments owing to the increased availability of remote sensing data for soil moisture retrieval (Ray et al., 2010; Brocca et al., 2016; Cullen et al., 2016; Zhuo et al., 2019). A study in central Italy showed that satellite-derived soil moisture outperforms antecedent precipitation in forecasting landslide movements (Brocca et al., 2012). A similar study is needed to evaluate the suitability of remotely sensed soil moisture for the assessment of rainfall-driven geohazards in other regions.

Rainfall thresholds are commonly established using rain gauge measurements. However, obtaining accurate rainfall data in mountainous regions is a major challenge (Guo et al., 2021). Several topographic factors, including altitude, slope, aspect, proximity to moisture sources, and exposure, affect the spatial distribution of rainfall (Al-Ahmadi and Al-Ahmadi, 2013). Significant discrepancies can exist in the observations of different gauges located a few kilometers apart (Krajewski et al., 2003; Gregoretti et al., 2016; Simoni et al., 2020). Because gauges are usually scarce in headwater regions, rainfall thresholds for debris flows are commonly derived from the observations of nearby gauges (Fan et al., 2018), which in the Alps, are typically located 4-15 km away from debris-flow sites, where dense networks of rain gauges are available (Nikolopoulos et al., 2014). This method tends to underestimate the rainfall that triggers debris flows (Abancó et al., 2016; Guo et al., 2021). Over the past three decades, remote sensing techniques, such as radar and satellites, have been used to provide rainfall estimates with increasing spatiotemporal resolution and accuracy (Brunetti et al., 2018). An example of this is the 10 km Integrated Multi-satellite Retrievals for the Global Precipitation Measurement (IMERG). Compared with ground-based rainfall radar networks, satellites can provide rainfall estimates at a global scale and can be used for areas with scarce ground data. Since the pioneering work of Hong et al. (2006), satellite-based rainfall data have been used for determining regional and global thresholds of rainfall-driven geohazards (Bhusan et al., 2014; Mathew et al., 2014; Kirschbaum and Stanley, 2018; Chikalamo et al., 2020; He et al., 2020; Jia et al., 2020; Abancó et al., 2021; Wang et al., 2021b; Li et al., 2022). A comparison between gauge-based and satellite-based thresholds revealed that the adjustment of satellite rainfall products (either gauge-based or by applying an error model) together with spatial resolution can improve the estimation of the rainfall thresholds (Nikolopoulos et al., 2017). In densely gauged areas, gauge-based thresholds outperform satellite-based thresholds (Brunetti et al., 2018), and viceversa in sparsely gauged regions (Brunetti et al., 2021). Considering that both gauge rainfall measurements and satellite observations have higher uncertainties in mountainous areas (Tan et al., 2017; Bulovic et al., 2020; Lu et al., 2021; Pradhan et al., 2022), comparing rainfall thresholds derived from different gauges and thresholds from satellite estimates at a local scale is beneficial for assessing the feasibility of satellite-based thresholds. However, such research studies have remained scarce.

Therefore, the aim of this study was to assess the potential of satellite-based rainfall and soil moisture estimates in determining the triggering conditions of debris flow in the Jiangjia Gully, which is an active debris-flow catchment. This area has a dense rain gauge network, and the debris-flow triggering therein is partly attributed to landslides (Yang et al., 2022). We first compared the characteristics of debris-flow-triggering rainfall derived from different rain gauge observations and rainfall estimates from the IMERG. We then defined the rainfall intensity-duration threshold for each rainfall dataset, and evaluated the performance of these thresholds using statistically based skill scores. Furthermore, as a third predictor variable, both satellite-based soil moisture (surface and root zone) and antecedent precipitation were tested.

2. Details of study location and datasets

2.1. Study location

The Jiangjia Gully is located in northeastern Yunnan Province of southern China and has a drainage area of 48.6 km². Debris flows are active in this watershed because of the erosion- and landslide-prone conditions, which are related to the presence of fractured bedrock, steep terrain (elevation of 1040–3260 m a.s.l.), and abundant moisture brought on by the summer monsoon. To study debris-flow activity in the watershed, the Chinese Academy of Sciences (CAS) in 1965, installed the Dongchuan Debris Flow Observation and Research Station (DDFORS). Since its establishment, >500 debris-flow events have been recorded, and each comprises tens or hundreds of surges (Guo et al., 2020).

The Menqian and Duozhao Gullies are the two largest tributaries, contributing 64.7% of the drainage area. Several check dams were built in the Duozhao Gully between 1979 and 1990, thereby greatly decreasing the debris-flow activity in this tributary. Currently, debris flows in the monitoring section of the main channel (Fig. 1) are primarily discharged from the Menqian Gully, which covers an area of 13.2 km². The exposed bedrock is fractured in the Jiangjia watershed and mostly disintegrates into particles of 20–100 mm. In addition, the basin is characterized by steep terrain, with 68% slopes of >25°. Gentler slopes are present close to the divides and are used as terraces. Both the fractured bedrock and the steep slopes facilitate an intense gully incision, which adds to the widespread development of landslides. Some landslides directly evolve into debris flows, whereas others release sediment into the channels, which is then mobilized by runoff (Yang et al., 2022).

The Jiangjia Gully located in the transition zone of the Indian summer monsoon and East Asian summer monsoon domains is characterized by a subtropical monsoon climate. The mean annual precipitation varies from 400 to 1000 mm and generally increases with elevation. Approximately 85% of the total annual rainfall occurs between May and October (Cui et al., 2005). Abundant rainfall in summer is the main contributor to the frequent episodes of debris flows (Guo et al., 2021).

2.2. Satellite data

The satellite rainfall data used in this study were obtained from the IMERG V06B product, which is available at https://gpm.nasa.gov/data/ directory. The IMERG algorithm integrates information from multiple sources, including satellite microwave precipitation estimates, infrared satellite estimates, and rain gauge analyses (Huffman et al., 2019). The IMERG has a pixel resolution of 0.1° (~ 10 km) and an interval of 30 min, spanning 60° N to 60° S. Several studies have found IMERG observations to be reliable in comparison to gauge or radar observations (Sahlu et al., 2016; Siuki et al., 2017; Salles et al., 2019; Thakur et al., 2019; Tang et al., 2020; Thakur et al., 2020; Sakib et al., 2021; Yu et al., 2021). The IMERG was run three times during each observation: an early run giving a quick estimate (latency of ~ 4 h), a late run with a better estimate owing to more data availability (latency of ~ 14 h), and a final run using monthly gauge data to create research-level products (latency of ~3.5 months). The early run product (IMERG-E) was used in this study because real-time precipitation data are needed for early warning

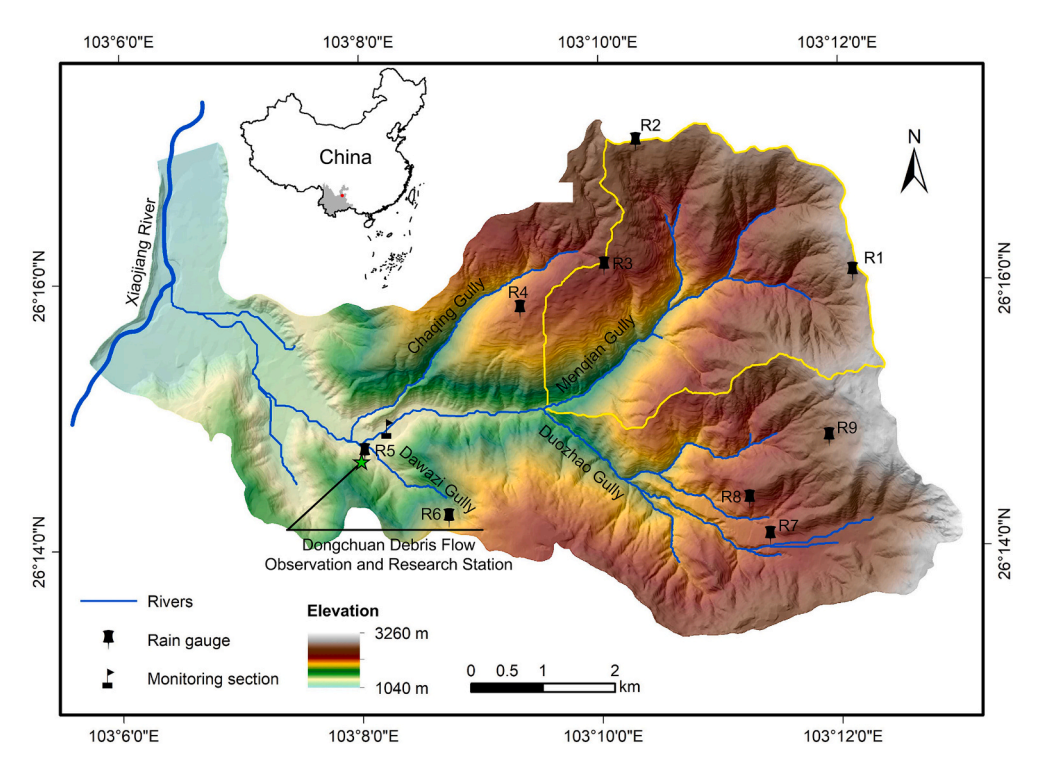


Fig. 1. Location and terrain of the Jiangjia Gully in northeastern Yunnan Province.

system of debris flow. In addition, the final run product (IMERG-F) was used for its superior performance (Zhou et al., 2021). Two IMERG grid cells covered the Jiangjia Gully, with percentages of 91.3% and 8.7%. We used rainfall estimates sampled from the major grid cell.

The satellite soil moisture data used in this study were obtained from the V06.1 product of the Climate Change Initiative program of the European Space Agency (CCI-SM), which can be accessed at https://data. ceda.ac.uk/neodc/esacci/soil_moisture/data. The CCI-SM merges active and passive microwave soil moisture products from multiple sensors, thereby providing global soil moisture estimates at a spatial resolution of 0.25° (~25 km) and a daily time step for the 1978–2020 period. Since its first release in 2012, product quality has steadily increased with each successive release (Dorigo et al., 2017). Several studies have evaluated the reliability of the CCI-SM using ground-based measurements, and the unbiased root mean square error is generally reported as 0.04 m³/m³ (Dorigo et al., 2015; An et al., 2016; Ma et al., 2019; Wang et al., 2021a). Four products are currently available: an active-microwave-based-only product, a passive-microwave-based-only product, a combined active-passive product, and an experimental breakadjusted product that attempts to reduce breaks in the combined product. For this study, the experimental break-adjusted product was used. Two CCI-SM pixels covered the study area, with percentages of 57.8% and 42.2%. We used the mean of the sampled estimates from these two pixels. Satellite sensors can only detect soil water content within the near-surface soil layer (<5 cm). However, shallow landslides typically involve soil mantles with thicknesses of 1-2 m (Fiorillo et al., 2001). Therefore, the exponential filter method described by Wagner et al. (1999) was used to derive root-zone soil moisture (SM-RZ) from nearsurface soil moisture:

$$SM - RZ(t) = \frac{\sum_{i} CCI - SM(t_i) \bullet exp\left(-\frac{(t-t_i)}{t_c}\right)}{\sum_{i} exp\left(-\frac{(t-t_i)}{t_c}\right)} \text{ for } t_i \le t$$
 (1)

where SM-RZ(t) is SM-RZ at time t, CCI-SM(t_i) is CCI-SM at time t_i, and t_c is the characteristic time length representing the time scale of soil moisture variation with depth. The suggested value of t_c is 20 days for

the 0-1 m soil layer.

2.3. Debris flow and rain gauge data

Debris flow and rain gauge data recorded during 2006–2010 in the Jiangjia Gully were used in this study due to the high incidence of debris flow and richness of rainfall data during this period. The CAS provided these data from the DDFORS. Table 1 shows the debris-flow catalogue demonstrating the exact time of occurrence for 32 debris-flow events and for one event only the occurrence date. All these events were observed in the monitoring section of the main channel (Fig. 1). The DDFORS staff manually recorded the debris-flow occurrence; the

Table 1
Occurrence times of debris-flow events triggered in the Jiangjia Gully during 2006–2010 (day/month/year hh:mm).

Number	Occurrence time	Number	Occurrence time	Number	Occurrence time
	5/7/2006		14/9/2007		5/8/2008
1	02:33	12	01:30	23	14:04
	6/7/2006		17/9/2007		8/8/2008
2	03:35	13	15:12	24	03:02
	15/8/2006		1/7/2008		11/8/2008
3	21:59	14	15:55	25	02:33
	20/8/2006		5/7/2008		17/8/2008
4	23:45	15	06:26	26	19:00
	10/7/2007		11/7/2008		4/8/2009
5	04:20	16	06:48	27	05:24
	24/7/2007		11/7/2008		6/7/2010
6	06:30	17	17:45	28	05:23
	25/7/2007		22/7/2008		17/7/2010
7	02:36	18	05:00	29	20:39
	25/7/2007		1/8/2008		22/7/2010
8	14:24	19	00:15	30	19:15
	30/7/2007		3/8/2008		24/7/2010
9	05:40	20	04:50	31	19:00
	11/8/2007		3/8/2008		5/8/2010
10	14:27	21	22:35	32	05:51
			4/8/2008		10/9/2010
11	25/8/2007	22	15:37	33	03:26

observation station was occupied only for 2–3 months during the monsoon period each year. This study refers to this period as the debrisflow observation period. The debris-flow observation periods in 2006–2010 included July 1–August 31 in 2006, July 1–September 17 in 2007, July 1–August 31 in 2008, July 1–August 31 in 2009, and July 1–September 10 in 2010.

Nine tipping bucket rain gauges were used during the study. Fig. 1 shows the locations of these gauges, which had elevations between 1346 and 2816 m. The gauges recorded the rainfall depth at an interval of 1 min. However, interrupted power supply and technical issues resulted in discontinuous measurements. Consequently, the period with available rainfall data varied from gauge to gauge, and Table 2 lists the specific measurement periods for each gauge. The 1-min gauge rainfall data were aggregated to half-hourly rainfall data to objectively compare the thresholds derived from the different rainfall data sources; thus, they had the same time interval as the satellite data. Since satellite observations act as an integrator over the area within one grid cell, the average of all rain gauge measurements (RA) was calculated and used as an additional dataset for a more realistic comparison.

3. Methods

3.1. Design for evaluating the feasibility of satellite rainfall product

The widely used power-law relationship between mean intensity (I) and rainfall duration (D), $I=aD^{-\beta}$, was used to represent the rainfall conditions for debris-flow occurrence. Dividing the long-term half-hourly rainfall sequences into individual events is essential for calculating I and D of a rainfall event. There are no standard criteria for separating rainfall time series (Jiang et al., 2021). In this study, a minimum time interval, $t_{\rm min}$, with a maximum rainfall depth, $P_{\rm max}$, was used to separate the rainfall events (Peres et al., 2018). Following the study of Zhou and Tang (2014), 6 h was selected for $t_{\rm min}$. $P_{\rm max}$ can be estimated as the potential evapotranspiration corresponding to $t_{\rm min}$ (Marino et al., 2020). In the study area, the mean daily potential evapotranspiration was approximately 4 mm during the rainy season. Thus, 1.0 mm was selected as the $P_{\rm max}$.

Rainfall events during the debris-flow observation periods were classified as debris-flow-triggering events (DFs) and non-triggering events (NDFs). When debris flows were triggered during a rainfall event or within 6 h ($t_{\rm min}$ used in this study) after the cessation of a rainfall event, the event was regarded as a DF. In general, it is impossible to divide rainfall conditions into a 100% debris-flow occurrence field and a 100% non-occurrence field. Therefore, we used logistic regression to determine the probabilistic rainfall thresholds of debris flow. In this approach, the probability of debris-flow occurrence (p) is expressed as a Sigmoid function of the linear combination of the explanatory variables:

$$ln\left(\frac{p}{1-p}\right) = a_0 + \sum_{i=1}^n a_i X_i \tag{2}$$

where a_i is the linear coefficient of the i^{th} predictor, X_i , and n is the

number of predictors. While deriving the I-D threshold, the predictors are ln(I) and ln(D):

$$ln\left(\frac{p}{1-p}\right) = a_0 + a_1 ln(I) + a_2 ln(D) \tag{3}$$

The equation can then be converted to the following forms:

$$ln(I) = \frac{ln(\frac{p}{1-p}) - a_0}{a_1} - \frac{a_2}{a_1}ln(D)$$
 (4)

$$I = exp\left(\frac{ln\left(\frac{p}{1-p}\right) - a_0}{a_1}\right) \bullet D^{-\frac{a_2}{a_1}}$$
 (5)

Comparing with the power-law relationship $I = \alpha D^{-\beta}$, α and β can be obtained as:

$$\alpha = exp\left(\frac{ln\left(\frac{p}{1-p}\right) - a_0}{a_1}\right) \tag{6}$$

$$\beta = \frac{a_2}{a_1} \tag{7}$$

The performance of the logistic regression model was evaluated using a receiver operating characteristic (ROC) analysis (Staley et al., 2013; Gariano et al., 2015; Giannecchini et al., 2016; Ju et al., 2020). First, different possible thresholds were given by assigning different p values in Eq. (6). For each threshold, the rainfall events were further classified into four groups: true positives (TP; DFs with rainfall conditions exceeding the threshold), false positives (FP; NDFs with rainfall conditions exceeding the threshold), true negatives (TN; NDFs with rainfall conditions below the threshold), and false negatives (FN; DFs with rainfall conditions below the threshold). The case of a debris-flow event without associated rainfall was also identified as an FN. It occurred either when the rainfall was considerably less to be defined as an event according to the criteria used in this study or when the rainfall was only measured by some of the gauges. To be distinguished from "normal" FN, this case was denoted as FN'. Second, the two skill scores, the probability of detection (POD) and probability of false detection (POFD), were calculated as follows for each threshold (Staley et al., 2013):

$$POD = \frac{TP}{TP + FN + FN'}$$
 (8)

$$POFD = \frac{FP}{FP + TN} \tag{9}$$

The perfect values for the two scores are 1 and 0, respectively. The POD obtained from each probabilistic threshold was plotted against the POFD to form an ROC curve. The area under this curve (AUC) varies between 0.5 (no improvement over random guessing) and 1.0 (perfect

Table 2
Time periods with available rainfall data for each rain gauge (R1–R9) and the gauge-averaged dataset (RA) in debris-flow observation periods during 2006–2010 (day/month).

Rain gauge	Elevation/m	2006	2007	2008	2009	2010	Available days
R1	2816	1/7-31/8	1/7–17/9	1/7-31/8	1/7-31/8	1/7-10/9	337
R2	2724	Null	1/7-17/9	1/7-31/8	1/7-31/8	1/7-19/8	253
R3	2325	Null	1/7-17/9	1/7-31/8	1/7-31/8	1/7-10/9	275
R4	2181	1/7-31/8	1/7-17/9	1/7-31/8	1/7-31/8	1/7-10/9	337
R5	1346	1/7-31/8	1/7-17/9	1/7-31/8	1/7-31/8	1/7-10/9	337
R6	1865	1/7-22/8	1/7-17/9	1/7-31/8	1/7-31/8	Null	256
R7	2230	Null	5/8-17/9	12/7-31/8	1/7-31/8	1/7-10/9	229
R8	2290	1/7-31/8	1/7-17/9	16/7-31/8	1/7-31/8	1/7-5/7	255
R9	2681	Null	1/7-17/9	1/7-31/8	1/7-31/8	15/8-10/9	230
RA		1/7-31/8	1/7-17/9	1/7-31/8	1/7-31/8	1/7-10/9	337

discrimination). We used AUC to evaluate the discriminatory power of different rainfall datasets in distinguishing DF from NDF conditions. The ROC curve indicates all possible thresholds and their relative balance between POD and POFD, and one is free to choose the optimal threshold depending on whether to maximize the POD or to minimize the POFD (Uwihirwe et al., 2022). To balance the two skill scores, we used the radial distance (RD) from the upper left corner of the ROC space (perfect classification point) to each (POFD, POD) data pair to select the optimal threshold (Gariano et al., 2015):

$$RD = \sqrt{(1 - POD)^2 + POFD^2}$$
 (10)

The perfect value for RD is 0. Therefore, the threshold with the minimum RD was defined as the optimal threshold. In addition to AUC, we used RD to evaluate the best-performing rainfall thresholds derived from different data sources.

3.2. Design for evaluating the feasibility of satellite soil moisture product

For each rainfall event, the satellite-based soil moisture with measurement time immediately prior to the onset of rainfall was identified. If the interval between the measurement time and the beginning of rainfall was <24 h (time step of the CCI-SM), the soil moisture was regarded as the initial moisture of the corresponding rainfall event. Unlike the IMERG data, which covered the entire study period, CCI-SM data for 46% of the study period were missing. Therefore, soil moisture data were only available for some of the rainfall events, which were used for further analysis.

Four cases were subjected to the logistic regression. In the first case, $\ln(I)$ and $\ln(D)$ were used as predictors as shown in Eq. (3). In other cases, antecedent precipitation (AP), CCI-SM, and SM-RZ were used as additional predictors. AP was calculated using the following equation (Bruce and Clark, 1966):

$$AP = \sum_{i=1}^{m} k^{i} P_{i} \tag{11}$$

where P_i is the rainfall depth measured in the $i^{\rm th}$ 24 h prior to the rainfall event, m is the number of days considered, and k is the decay factor. The suggested values for m and k are 7 and 0.84, respectively (Yang et al., 2020). To determine whether the original or the logarithmic form of AP, CCI-SM, and SM-RZ should be used, the statistical significance of each form was evaluated with the Wald test, which is a hypothesis test performed on the parameters calculated by the maximum likelihood estimation, using the corresponding form as the single explanatory variable in the logistic regression. The more significant form was selected.

The performance of the thresholds defined in different cases was also

evaluated using the AUC and the RD of the optimal threshold. Because of the incomplete soil moisture data in the debris-flow observation periods, nearly half of the DFs had no associated information. Treating these cases as FN' would result in a much smaller POD score. Therefore, FN' was removed from Eq. (8) when the satellite soil moisture product was evaluated.

4. Results

4.1. Characteristics of DFs

Fig. 2 shows the distribution of D and I in the DFs in the Jiangjia Gully according to the gauge observations and IMERG. D fluctuated from 0.5 to 56.5 h, whereas I varied between 0.39 and 16.67 mm/h. However, the 75th percentiles for D and I were smaller than 15 h and 7.5 mm/h, respectively. The calculated distributions of D and I differed from gauge to gauge, indicating notable spatial heterogeneity in the rainfall of the study area. Compared with the rain gauge data, both the IMERG-E and IMERG-F generally overestimated the rainfall duration and underestimated the mean intensity. For instance, Fig. 3 illustrates the rainfall time series on August 11, 2007 in each dataset; the D and I calculated from gauge observations ranged from 2.5 to 6.0 h and from 2.13 to 6.37 mm/h, while D was >15 h and I was approximately 1.00 mm/h, according to the IMERG data.

4.2. Performance of the I-D thresholds derived from different rainfall datasets

Table 3 lists the number of DFs and NDFs for each rainfall dataset: their sum is the total number of rainfall events in the debris-flow observation periods during 2006-2010. Rainfall datasets from the R1, R4, R5, RA, and IMERG were complete in the observation periods and therefore were comparable. The gauge installed at the highest elevation (i.e. R1) detected the highest number of rainfall events (141), whereas the gauge installed in the valley (i.e. R5) detected the lowest number of rainfall events (100), indicating that some rainfall events occurred only in the headwater regions. Furthermore, the probabilistic thresholds derived from the gauges located in the main active tributary (i.e. R1–R3) had higher AUC values than those derived from the other gauges, except R4. These gauges detected nearly all DFs, with FN' equivalent to 0 or 1. In contrast, at least two DFs were not detected by the other gauges, except R4. This may account for the difference in the AUC values. For RA, FN' was equivalent to 0 and the AUC was high. Although the total number of rainfall events derived from the IMERG-E (138) and IMERG-F (132) was nearly equal to that of RA (133), 5-6 DFs were not detected by them. In addition, a large number of FP and FN were present; thus the

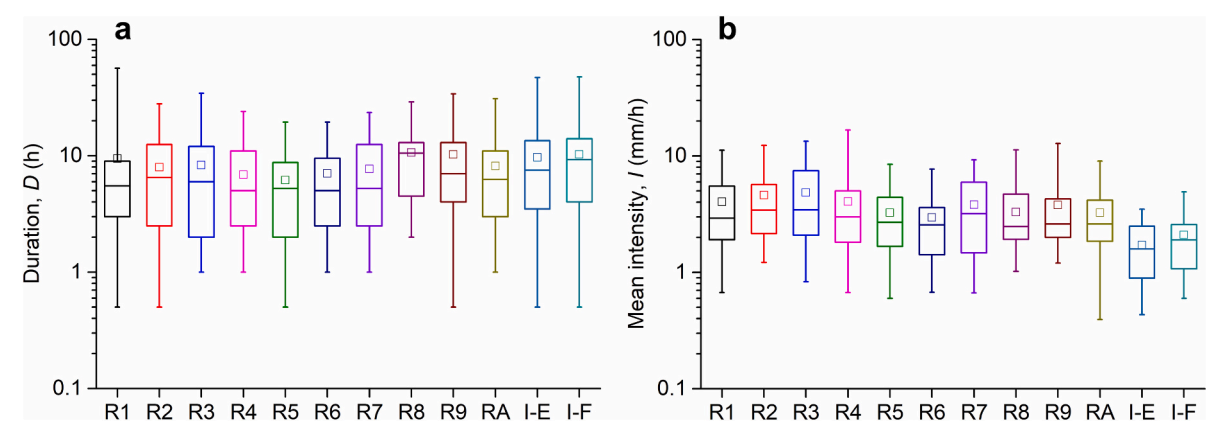


Fig. 2. Box-Whisker plots showing the distribution of (a) duration and (b) mean intensity of DFs according to rain gauge observations (R1–R9 and RA) and satellite-based estimates. I-E and I-F represent IMERG-E and IMERG-F, respectively. The whiskers extend from the minimum to the maximum. The bottom and top edges of the box indicate the 25th and 75th percentiles. The middle line and the square show the median and mean.

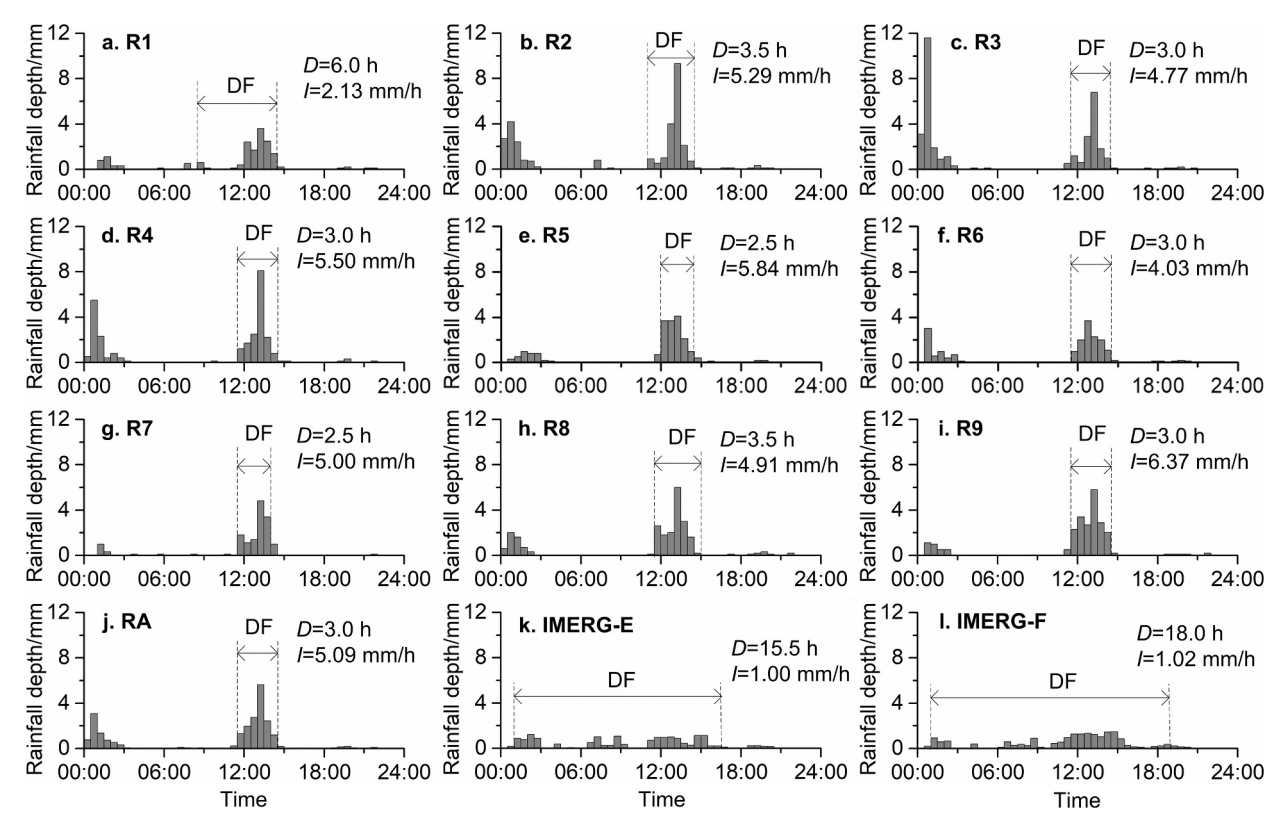


Fig. 3. Half-hourly rainfall time series measured by the gauges (R1–R9 and RA) and IMERG on August 11, 2007. A debris flow event was detected at 14:27 in the monitoring section of the main channel. Characteristics of the associated rainfall event (DF) are presented.

Table 3Performance of the *I-D* thresholds derived from rain gauge measurements (R1–R9 and RA) and satellite-based rainfall estimates (IMERG-E and IMERG-F).

Rainfall	Number of rainfall events			FN'	AUC	Optima	al threshold
dataset	DFs	NDFs	Total			RD	Threshold
R1	30	111	141	1	0.785	0.349	$I = 11.20D^{-1.00}$
R2	26	75	101	1	0.860	0.238	$I = 9.58D^{-0.86}$
R3	28	77	105	0	0.836	0.361	$I = 8.93D^{-0.80}$
R4	31	83	114	1	0.854	0.289	$I = 6.86D^{-0.75}$
R5	28	72	100	4	0.686	0.425	$I = 6.08D^{-0.80}$
R6	21	56	77	5	0.681	0.396	$I = 8.78D^{-1.14}$
R7	18	66	84	2	0.754	0.405	$I = 5.83D^{-0.99}$
R8	19	76	95	3	0.772	0.322	$I = 13.86D^{-0.98}$
R9	21	69	90	2	0.742	0.379	$I = 12.46D^{-0.98}$
RA	32	101	133	0	0.860	0.284	$I = 5.96D^{-0.74}$
IMERG-E	25	113	138	6	0.579	0.532	$I = 70.67D^{-2.24}$
IMERG-F	26	106	132	5	0.624	0.511	$I = 6.14D^{-0.99}$

AUC was smaller than that of the gauge observations.

The optimal threshold derived from each dataset is listed in Table 3 and presented in Fig. 4. The thresholds derived from the gauge data exhibited great variability, with α and β varying in the ranges 5.83–13.86 and 0.74–1.14, respectively. This indicates that a rainfall threshold from one gauge cannot simply be applied to another one, i.e. that it is crucial to fit the threshold to the characteristics of one rain gauge observation. The RD values of these thresholds were between 0.238 and 0.425, with the minimum value obtained by R2, which also had the maximum AUC. The parameters α and β defined by the IMERG-E were 70.67 and 2.24, respectively, and were much higher than the gauge-based threshold parameters. In contrast, the two parameters

defined by the IMERG-F were 6.14 and 0.99, respectively, and were within the range of gauge-based threshold parameters. Compared with the threshold parameters of RA, their relative differences were 3% and 35%, respectively. These results show the feasibility of IMERG-F in determining thresholds. However, the RD was 0.511, which was considerably higher than that of the gauge-based thresholds. Therefore, the IMERG-F was weaker than the gauge measurements in terms of the discriminatory power to distinguish DF from NDF conditions.

4.3. Performance of thresholds including initial soil wetness conditions

Table 4 lists the p-values of the Wald test when using the AP, CCI-SM, and SM-RZ or their logarithms as the single explanatory variable in the logistic regression. For all rainfall datasets, the *p*-value using ln(AP) was smaller than that using AP, whereas the p-values using ln(CCI-SM) and ln(SM-RZ) were comparable to the values using CCI-SM and SM-RZ, respectively. Therefore, for simplicity, ln(AP), CCI-SM, and SM-RZ were separately used as the third predictor in addition to ln(I) and ln(D) in the logistic regression. The AUC of the probabilistic thresholds and RD of the optimal threshold were calculated for each rainfall dataset and compared with the case where only ln(I) and ln(D) were used as predictors (reference case), as illustrated in Fig. 5. Overall, the inclusion of ln(AP) in the logistic regression generally performed better than the reference case. The average increase was 0.033 for the AUC and the average decrease was 0.028 for the RD. The inclusion of the CCI-SM had little influence on logistic regression performance. The inclusion of the SM-RZ increased the average RD by 0.012 and increased the average AUC by 0.007. Therefore, after including the SM-RZ, the overall performance was similar to that of the reference case.

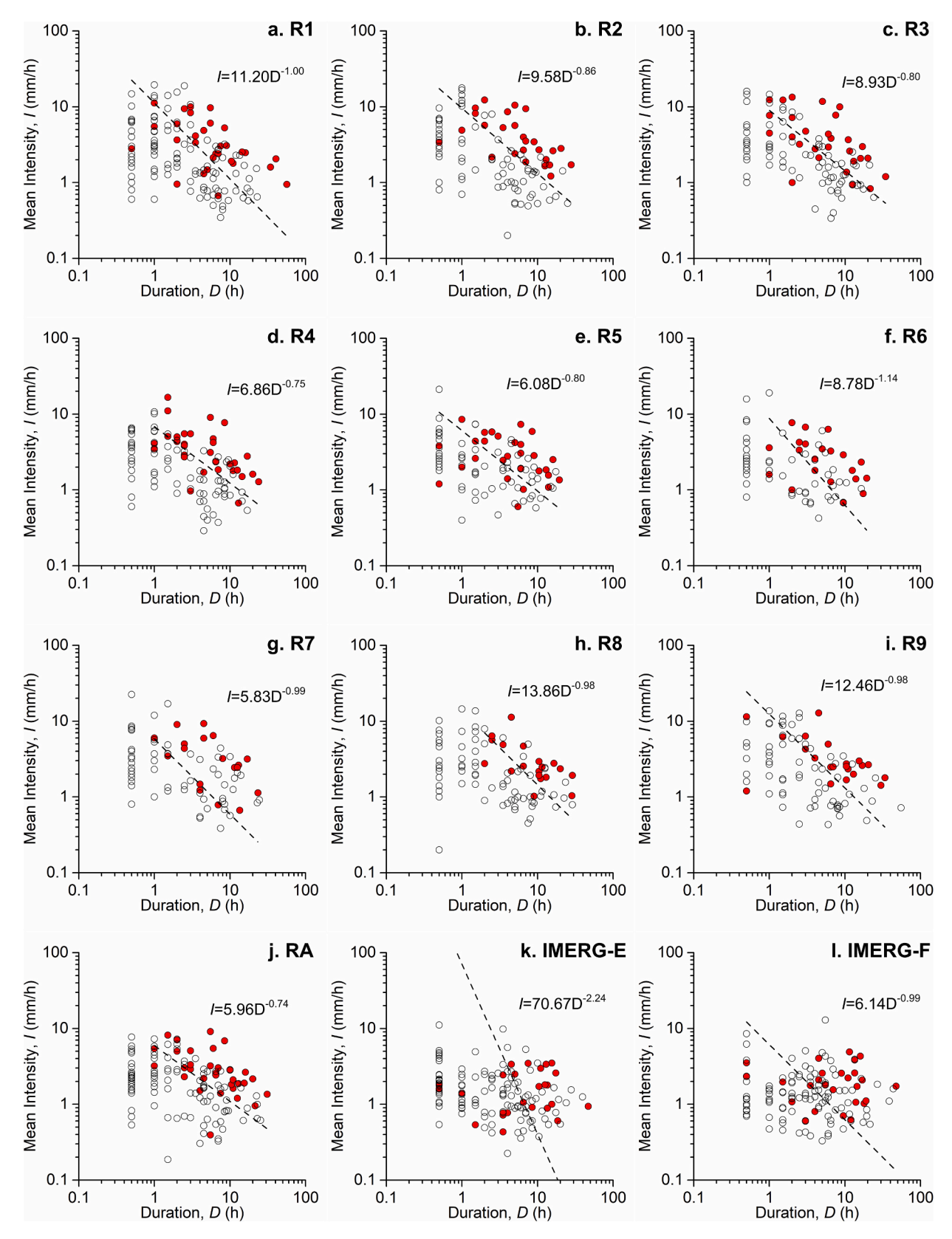


Fig. 4. Mean intensity versus duration of DFs (red solid circles) and NDFs (hollow circles) and the optimal thresholds (dashed line) derived from different rainfall datasets. (For interpretation of the references to colour in this figure legend, the reader is referred to the web version of this article.)

Table 4
p-values of the Wald test when antecedent precipitation (AP), satellite-based surface and root-zone soil moisture (CCI-SM and SM-RZ) or their logarithms were used as the single explanatory variable in the logistic regression. Rainfall events used in this table are a subset of those shown in Table 3.

Rainfall dataset	Number of rainfall events			Explanatory variable						
	DFs	NDFs	Total	AP	ln(AP)	CCI-SM	ln(CCI-SM)	SM-RZ	ln(SM-RZ)	
R1	18	52	70	0.091	0.051	0.777	0.842	0.815	0.812	
R2	16	43	59	0.029	0.025	0.651	0.756	0.477	0.465	
R3	19	43	62	0.040	0.023	0.581	0.638	0.824	0.812	
R4	19	37	56	0.644	0.260	0.532	0.585	0.723	0.727	
R5	16	34	50	0.355	0.196	0.472	0.441	0.320	0.318	
R6	11	30	41	0.218	0.212	0.438	0.405	0.041	0.042	
R7	13	36	49	0.566	0.163	0.087	0.104	0.769	0.770	
R8	12	32	44	0.126	0.083	0.896	0.793	0.089	0.091	
R9	14	41	55	0.153	0.061	0.847	0.907	0.203	0.205	
RA	19	47	66	0.105	0.046	0.596	0.673	0.909	0.917	
IMERG-E	14	65	79	0.912	0.722	0.947	0.888	0.992	0.999	
IMERG-F	16	53	69	0.317	0.196	0.757	0.778	0.472	0.461	

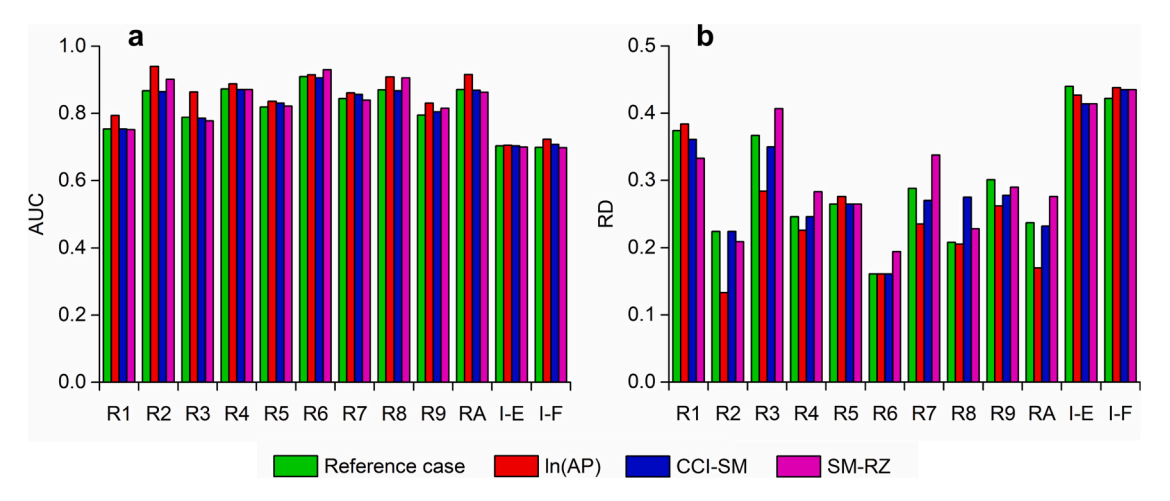


Fig. 5. Comparison of (a) AUC and (b) minimum RD when antecedent precipitation (AP), satellite-based surface and root-zone soil moisture (CCI-SM and SM-RZ) were used as the third predictor in the logistic regression with the case wherein only ln(I) and ln(D) were used (reference case). I-E and I-F represent IMERG-E and IMERG-F, respectively.

5. Discussion

5.1. Feasibility of the IMERG-F in the threshold definition of debris flow

The optimal rainfall threshold of debris flow in the Jiangjia Gully defined by the IMERG-F was comparable to that defined by the rain gauge data measured in the watershed. Nonetheless, the smaller AUC and greater RD values indicate that the performance of the threshold was poorer. Therefore, gauge measurements are preferable for gauged debris-flow watersheds. For ungauged watersheds, the suitability of the datasets—satellite-based estimates or gauge measurements from the

Table 5Statistical metrics during comparison of half-hourly rainfall depth measured by the different gauges and IMERG with the data recorded by gauge R2.

Rainfall dataset	CC	MB/mm	MAE/mm	RMSE/mm
R1	0.650	0.008	0.080	0.545
R3	0.789	0.001	0.057	0.407
R4	0.715	-0.026	0.062	0.460
R5	0.525	-0.044	0.078	0.561
R6	0.474	-0.040	0.082	0.595
R7	0.565	-0.016	0.090	0.569
R8	0.637	0.000	0.082	0.535
R9	0.626	0.014	0.087	0.572
RA	0.829	-0.012	0.056	0.379
IMERG-E	0.232	-0.025	0.125	0.664
IMERG-F	0.310	0.000	0.133	0.678

surrounding areas must be decided. To this end, we assumed that the rainfall characteristics measured by gauge R2, which provided the best AUC and RD values, represented the "true" DF characteristics. We then compared the half-hourly rainfall depth measured by the different gauges and IMERG with the data recorded by gauge R2, in the overlapping periods listed in Table 2, that is, August 5-September 17 in 2007, July 16-August 31 in 2008, and July 1-August 31 in 2009. Statistical metrics including the Pearson's correlation coefficient (CC), mean bias (MB), mean absolute error (MAE), and root mean square error (RMSE) were calculated and their values are listed in Table 5. Among these metrics, the CC had the strongest correlation with the AUC and RD values listed in Table 3, with p < 0.001. Additionally, we calculated the CC between the half-hourly rainfall depths measured by each pair of gauges. The results showed that the CC was negatively correlated with the horizontal distance (HD) between the two corresponding gauges. Fig. 6 shows that the CC between the half-hourly gauge-measured rainfall depth and IMERG-F data was also negatively correlated with the HD between the corresponding gauge and the center of the $0.1^{\circ} \times 0.1^{\circ}$ grid cell used to extract rainfall data in the IMERG-F. The distance between the headwater region of a debris-flow watershed and the center of the nearest grid cell of an IMERG-F varies from 0 to approximately 7 km. Using the fitting line between the HD and CC for the gauge versus the IMERG-F case in Fig. 6 (i.e. CC = 0.4257-0.0279HD), the CC varied between 0.228 and 0.426, which corresponded to distances 6.9-9.7 km of the fitting line between the HD and CC for the gauge versus gauge case (i.e. CC = 0.9111-0.0703HD). This suggests that when the nearest rain

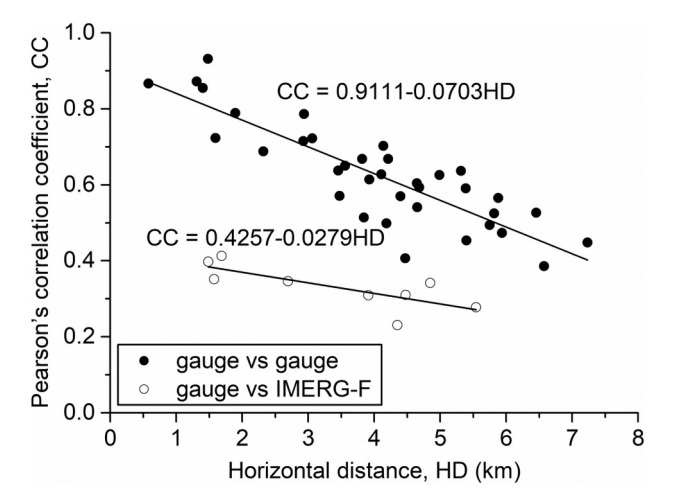


Fig. 6. Scatter plots of Pearson's correlation coefficient (CC) between half-hourly rainfall depth of each pair of gauges versus the horizontal distance (HD) between the corresponding gauges, and scatter plots of CC between the half-hourly gauge-measured rainfall depth and IMERG-F data versus the HD between the corresponding gauge and center of the $0.1^{\circ} \times 0.1^{\circ}$ grid cell used to extract the rainfall data in the IMERG-F.

gauge is located farther than 10 km from the headwater region of a debris-flow basin, the IMERG-F is expected to provide better rainfall threshold estimates. This result is consistent with the work of Brunetti et al. (2018, 2021)), who reported that in comparison to satellite-based data with a spatial resolution of 10 km, gauge-based rainfall datasets are better at identifying landslide occurrences when they have an equivalent spatial resolution; the opposite is true when gauge-based data have a spatial resolutions of 25 km. However, concerning the complexity of rainfall field in mountainous regions, the distance obtained in this study is only valid for the study site and needs to be reassessed for other regions.

5.2. Factors influencing the feasibility of CCI-SM in the threshold definition of debris flow

Compared to using the AP, the use of the CCI-SM and SM-RZ for defining the threshold of debris flow was inferior for the study area. To investigate the reasons for this result, daily soil moisture and gauge-averaged rainfall depth from June to September in 2007 were analyzed as a case study, as illustrated in Fig. 7. The CCI-SM varied between 0.285 and 0.417 $\rm m^3/m^3$, whereas the SM-RZ varied between 0.335 and 0.380 $\rm m^3/m^3$ during the investigation period. Overall, the CCI-SM was sensitive to rainfall; it decreased with no rain gaps and increased or stabilized during rainy days. However, the opposite was observed at times. For instance, the CCI-SM decreased by 0.042 $\rm m^3/m^3$

from July 24 to July 25, although the rainfall depth surpassed 30 mm on both the days, and it increased by 0.024 m³/m³ from August 5 to August 6, although it did not rain on these two days. This was most likely induced by the measurement error in the CCI-SM, which has a typical value of $0.04 \text{ m}^3/\text{m}^3$ (Dorigo et al., 2017). Additionally, the thin nearsurface layer of soil can be saturated by small rainfall events. Specifically, as shown in Fig. 8, the CCI-SM remained approximately 0.4 m³/ m³ when the rainfall depth accumulated within 24 h before soil moisture detection exceeded ~3 mm. Moreover, the pixel resolution of the CCI-SM (~25 km) was much coarser compared to the drainage area of the Jiangjia Gully (48.6 km²). Considering the significant spatial heterogeneity of soil moisture in mountainous terrains induced by the spatial variability in soil texture, vegetation, topography, and meteorological factors (Li et al., 2022), a spatial-scale mismatch may generate a notable error. In addition, the temporal resolution of the CCI-SM (1 d) was coarse compared with the minimum time interval (6 h) used to separate the rainfall events in this study. For a given rainfall event, the available soil moisture might have been detected before an event that occurred prior to this event. In such a case, the available soil moisture tended to underestimate the initial soil wetness during this event. Fig. 7 reveals that the SM-RZ had the same tendency of change as CCI-SM, although it was not sensitive to random measurement errors in the CCI-SM. For instance, the decrease in the SM-RZ from July 24 to July 25 and the increase from August 5 to August 6 were <0.001 m³/m³. However, limitations in the spatiotemporal resolution remained. In addition, the change in the SM-RZ was small when the CCI-SM remained high. For instance, the increase in the SM-RZ was 0.014 m³/m³ during July

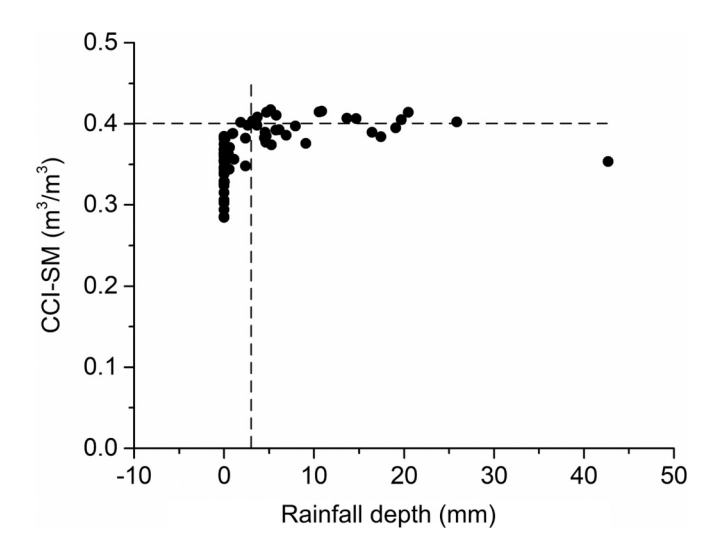


Fig. 8. Scatter plots of satellite-based surface soil moisture (CCI-SM) versus rainfall depth accumulated within the 24 h before soil moisture detection.

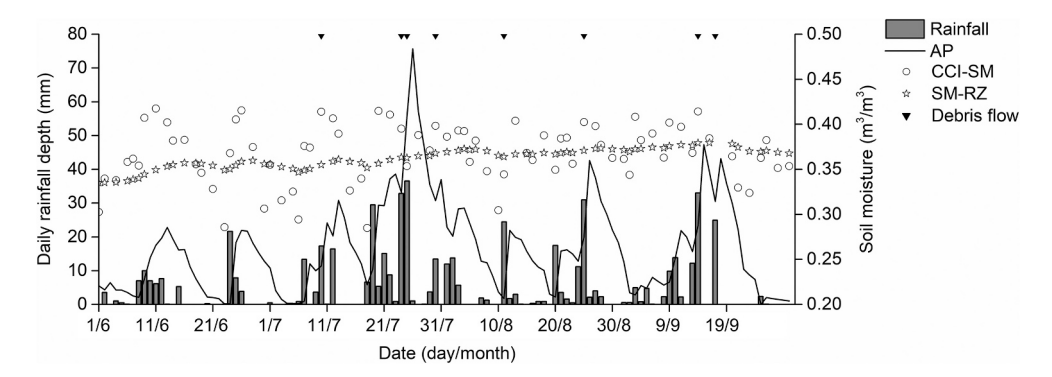


Fig. 7. Gauge-averaged daily rainfall depth, antecedent precipitation (AP), and satellite-based surface and root-zone soil moisture (CCI-SM and SM-RZ) during June–September in 2007.

20–August 3, whereas the total rainfall depth was 143.2 mm in the corresponding period. This could make the SM-RZ insensitive to extreme rainfall events. These are likely the main reasons for the poorer performance of the SM-RZ compared with that of the AP.

5.3. Uncertainties in the threshold determination

The rapid rise of satellite rainfall products provide opportunities for researchers to access more available data to study the triggering conditions of rainfall-driven hazards. This study took advantage of these opportunities by comparing satellite-based rainfall thresholds with gauge-based thresholds for debris flow. However, uncertainties in the threshold determination were not considered during comparison. Firstly, uncertainties can stem from the division of rainfall time series into individual events. Generally, a minimum inter-event duration (t_{min}) was used to separate two contiguous rainfall events. For studying debris flow, values from 10 min (Coe et al., 2008) to 7 h (Jiang et al., 2021) have been used for t_{min} in the literature. Bel et al. (2017) showed that selecting t_{min} has a strong impact on the definition of rainfall threshold as it influences the event starting and ending time. In addition, uncertainties exist in the linear coefficients associated with logistic regression. For instance, the regression coefficients in Eq. (3) for the IMERG-F were $\alpha_1 = 0.742$ and $\alpha_2 = 0.736$, with a standard error of 0.346 and 0.231, respectively. The resulting uncertainty in β was $\pm 0.231/$ 0.742 (i.e. ± 0.31). Furthermore, the optimal threshold may vary when the performance matric used for selection is changed. For instance, the optimal rainfall threshold derived from the IMERG-F would be I =10.72D^{-0.99} if the Hanssen-Kuiper skill score, which is defined as the difference between POD and POFD, is maximized. Thus, further research is needed to comprehensively estimate the uncertainties in the rainfall threshold to achieve a more rigorous evaluation of the feasibility of satellite rainfall products in defining the triggering conditions of debris flow.

6. Conclusion

In this study, using the IMERG-E, IMERG-F and CCI-SM, we evaluated the feasibility of satellite-based precipitation and soil moisture data for determining the thresholds for triggering debris flow at the local scale. The rainfall properties of DFs derived from different rain gauges and satellite estimates exhibited great variability, resulting in considerable differences in the I-D thresholds. Overall, the thresholds defined from the gauge data measured in the initiation zone of debris flow performed better than those defined from the data recorded in other parts of the watershed. This was primarily because more DFs were detected. The I-D threshold determined by the IMERG-E deviated from the gauge-based thresholds. Although the threshold derived from the IMERG-F was comparable to the gauge-based ones, the presence of substantial FN and FP indicated that performance of the IMERG-F was weaker. Therefore, rain gauge measurements are preferred for determining threshold in gauged watersheds. For ungauged watersheds, the IMERG-F is suitable when the nearest available gauge is farther than 10 km from the initiation zone of the debris flow. Because debris-flow occurrence is partly attributed to the triggering of landslides in the study basin, the initial soil wetness status is expected to impact the rainfall conditions for debris-flow triggering. We found that the performance of the thresholds improved when the AP was included in the threshold definition. Adding the CCI-SM to the threshold definition had little impact on the performance of the thresholds because of measurement error, ease of saturation, and relatively coarse spatiotemporal resolutions. The spatial variabilities in rainfall and soil wetness are commonly large in debris-flow-prone regions with complex topography. Therefore, these results are only valid for the study catchment and still need to be validated or assessed for other catchments or regions. In addition, various downscaling techniques have been studied for satellite soil moisture products during recent decades. These techniques provide a solution to the aforementioned resolution issue. Further research is needed to assess the feasibility using these techniques to obtain satellite-based soil moisture data to determine the triggering conditions for debris flow.

CRediT authorship contribution statement

Hongjuan Yang: Conceptualization, Methodology, Writing – original draft. Kaiheng Hu: Conceptualization, Supervision, Funding acquisition. Shaojie Zhang: Writing – review & editing. Shuang Liu: Writing – review & editing.

Declaration of Competing Interest

The authors declare that they have no known competing financial interests or personal relationships that could have appeared to influence the work reported in this paper.

Data availability

Data will be made available on request.

Acknowledgements

Dongchuan Debris Flow Observation and Research Station, Chinese Academy of Sciences is acknowledged for ground-based data supply. This research was supported by the Second Tibetan Plateau Scientific Expedition and Research Program (Grant No. 2019QZKK0902), the National Natural Science Foundation of China (Grant No. 91747207), the National Key R&D Program of China (Grant No. 2018YFC1505205), and the Dadu River Research Project (Grant No. KB-KY-2021-001). We are grateful to the two anonymous reviewers for their valuable comments and suggestions.

References

- Abancó, C., Hürlimann, M., Moya, J., Berenguer, M., 2016. Critical rainfall conditions for the initiation of torrential flows. Results from the Rebaixader catchment (Central Pyrenees). J. Hydrol. 541, 218–229.
- Abancó, C., Bennett, G.L., Matthews, A.J., Matera, M.A.M., Tan, F.J., 2021. The role of geomorphology, rainfall and soil moisture in the occurrence of landslides triggered by 2018 Typhoon Mangkhut in the Philippines. Nat. Hazards Earth Syst. Sci. 21, 1531–1550.
- Al-Ahmadi, K., Al-Ahmadi, S., 2013. Rainfall-altitude relationship in Saudi Arabia. Adv. Meteorol. 2013, 363029.
- An, R., Zhang, L., Wang, Z., Quaye-Ballard, J.A., You, J., Shen, X., Gao, W., Huang, L., Zhao, Y., Ke, Z., 2016. Validation of the ESA CCI soil moisture product in China. Int. J. Appl. Earth Obs. 48, 28–36.
- Badoux, A., Graf, C., Rhyner, J., Kuntner, R., McArdell, B.W., 2009. A debris-flow alarm system for the Alpine Illgraben catchment: design and performance. Nat. Hazards 49, 517–539.
- Bel, C., Liébault, F., Navratil, O., Eckert, N., Bellot, H., Fontaine, F., Laigle, D., 2017. Rainfall control of debris-flow triggering in the Réal Torrent, Southern French Prealps. Geomorphology 291, 17–32.
- Bhusan, K., Kundu, S.S., Goswami, K., Sudhakar, S., 2014. Susceptibility mapping and estimation of rainfall threshold using space based input for assessment of landslide hazard in Guwahati city in North East India. Int. Arch. Photogramm. Remote. Sens. Spat. Inf. Sci. 40, 15–19.
- Brocca, L., Ponziani, F., Moramarco, T., Melone, F., Berni, N., Wagner, W., 2012. Improving landslide forecasting using ASCAT-derived soil moisture data: a case study of the Torgiovannetto landslide in Central Italy. Remote Sens. 4, 1232–1244.
- Brocca, L., Ciabatta, L., Moramarco, T., Ponziani, F., Berni, N., Wagner, W., 2016. Chapter 12-use of satellite soil moisture products for the operational mitigation of landslides risk in Central Italy. In: Srivastava, P.K., Petropoulos, G.P., Kerr, Y.H. (Eds.), Satellite Soil Moisture Retrieval. Elsevier, pp. 231–247.
- Bruce, J.P., Clark, R.H., 1966. Introduction to Hydrometeorology. Pergamon, Oxford. Brunetti, M.T., Melillo, M., Peruccacci, S., Ciabatta, L., Brocca, L., 2018. How far are we from the use of satellite rainfall products in landslide forecasting? Remote Sens. Environ. 210, 65–75.
- Brunetti, M.T., Melillo, M., Gariano, S.L., Ciabatta, L., Brocca, L., Amarnath, G., Peruccacci, S., 2021. Satellite rainfall products outperform ground observations for landslide prediction in India. Hydrol. Earth Syst. Sci. 25, 3267–3279.
- Bulovic, N., McIntyre, N., Johnson, F., 2020. Evaluation of IMERG V05B 30-min rainfall estimates over the high-elevation tropical Andes Mountains. J. Hydrometeorol. 21 (12), 2875–2892.

H. Yang et al. Engineering Geology 315 (2023) 107041

Chikalamo, E.E., Mavrouli, O.C., Ettema, J., van Westen, C.J., Muntohar, A.S., Mustofa, A., 2020. Satellite-derived rainfall thresholds for landslide early warning in Bogowonto Catchment, Central Java, Indonesia. Int. J. Appl. Earth Obs. 89, 102093.

- Coe, J.A., Kinner, D.A., Godt, J.W., 2008. Initiation conditions for debris flows generated by runoff at Chalk Cliffs, central Colorado. Geomorphology 96, 270–297.
- Cui, P., Chen, X., Wang, Y., Hu, K., Li, Y., 2005. Jiangjia Ravine debris flows in south-western China. In: Jakob, M., Hungr, O. (Eds.), Debris-flow Hazards and Related Phenomena. Springer, Berlin, pp. 565–594.
- Cullen, C.A., Al-Suhili, R., Khanbilvardi, R., 2016. Guidance index for shallow landslide hazard analysis. Remote Sens. 8, 866.
- Deganutti, A.M., Marchi, L., Arattano, M., 2000. Rainfall and debris flow occurrence in the Moscardo basin (Italian Alps). In: Wieczorek, G.F., Naeser, N.D. (Eds.), Debris-Flow Hazards Mitigation: Mechanics, Prediction, and Assessment. Balkema, Rotterdam, pp. 67–72.
- Dorigo, W.A., Gruber, A., De Jeu, R.A.M., Wagner, W., Stacke, T., Loew, A., Albergel, C., Brocca, L., Chung, D., Parinussa, R.M., Kidd, R., 2015. Evaluation of the ESA CCI soil moisture product using ground-based observations. Remote Sens. Environ. 162, 280, 205
- Dorigo, W., Wagner, W., Albergel, C., Albrecht, F., Balsamo, G., Brocca, L., Chung, D., Ertl, M., Forkel, M., Gruber, A., Haas, E., Hamer, P.D., Hirschi, M., Ikonen, J., de Jeu, R., Kidd, R., Lahoz, W., Liu, Y.Y., Miralles, D., Mistelbauer, T., Nicolai-Shaw, N., Parinussa, R., Pratola, C., Reimer, C., van der Schalie, R., Seneviratne, S.I., Smolander, T., Lecomte, P., 2017. ESA CCI Soil Moisture for improved Earth system understanding: State-of-the art and future directions. Remote Sens. Environ. 203, 185-215
- Dowling, C.A., Santi, P.M., 2014. Debris flows and their toll on human life: a global analysis of debris-flow fatalities from 1950 to 2011. Nat. Hazards 71, 203–227.
- Fan, R.L., Zhang, L.M., Wang, H.J., Fan, X.M., 2018. Evolution of debris flow activities in Gaojiagou Ravine during 2008-2016 after the Wenchuan earthquake. Eng. Geol. 235, 1–10.
- Fiorillo, F., Guadagno, F., Aquino, S., De Blasio, A., 2001. The December 1999 Cervinara landslides: further debris flows in the pyroclastic deposits of Campania (southern Italy). B Eng. Geol. Environ. 60, 171–184.
- Garcia-Urquia, E., 2016. Establishing rainfall frequency contour lines as thresholds for rainfall-induced landslides in Tegucigalpa, Honduras, 1980-2005. Nat. Hazards 82, 2107–2132.
- Gariano, S.L., Brunetti, M.T., Iovine, G., Melillo, M., Peruccacci, S., Terranova, O., Vennari, C., Guzzetti, F., 2015. Calibration and validation of rainfall thresholds for shallow landslide forecasting in Sicily, southern Italy. Geomorphology 228, 653–665.
- Giannecchini, R., Galanti, Y., Avanzi, G.D., Barsanti, M., 2016. Probabilistic rainfall thresholds for triggering debris flows in a human-modified landscape. Geomorphology 257, 94–107.
- Gregoretti, C., Degetto, M., Bernard, M., Crucil, G., Pimazzoni, A., De Vido, G., Berti, M., Simoni, A., Lanzoni, S., 2016. Runoff of small rocky headwater catchments: Field observations and hydrological modeling. Water Resour. Res. 52 (10), 8138–8158.
- Guo, X., Li, Y., Cui, P., Yan, H., Zhuang, J., 2020. Intermittent viscous debris flow formation in Jiangjia Gully from the perspectives of hydrological processes and material supply. J. Hydrol. 589, 125184.
- Guo, X., Cui, P., Chen, X., Li, Y., Zhang, J., Sun, Y., 2021. Spatial uncertainty of rainfall and its impact on hydrological hazard forecasting in a small semiarid mountainous watershed. J. Hydrol. 595, 126049.
- Hawke, R., McConchie, J., 2011. In situ measurement of soil moisture and pore-water pressures in an 'incipient' landslide: Lake Tutira, New Zealand. J. Environ. Manag. 92, 266–274.
- He, S., Wang, J., Liu, S., 2020. Rainfall event–duration thresholds for landslide occurrences in China. Water 12, 494.
- Hirschberg, J., Badoux, A., McArdell, B.W., Leonarduzzi, E., Molnar, P., 2021. Evaluating methods for debris-flow prediction based on rainfall in an Alpine catchment. Nat. Hazards Earth Syst. Sci. 21, 2773–2789.
- Hong, Y., Adler, R., Huffman, G., 2006. Evaluation of the potential of NASA multisatellite precipitation analysis in global landslide hazard assessment. Geophys. Res. Lett. 33, L22402.
- Huffman, G.J., Bolvin, D.T., Braithwaite, D., Hsu, K., Joyce, R., Kidd, C., Nelkin, E.J., Sorooshian, S., Tan, J., Xie, P., 2019. NASA Global Precipitation Measurement (GPM) Integrated Multi-satellitE Retrievals for GPM (IMERG). NASA/GSFC, Greenbelt, MD, USA.
- Iverson, R.M., 1997. The physics of debris flows. Rev. Geophys. 35 (3), 245–296.Iverson, R.M., Reid, M.E., Lahusen, R.G., 1997. Debris-flow mobilization from landslides.Annu. Rev. Earth Planet. Sci. 25, 85–136.
- Jia, G., Tang, Q., Xu, X., 2020. Evaluating the performances of satellite-based rainfall data for global rainfall-induced landslide warnings. Landslides 17, 283–299.
- Jiang, Z., Fan, X., Subramanian, S.S., Yang, F., Tang, R., Xu, Q., Huang, R., 2021. Probabilistic rainfall thresholds for debris flows occurred after the Wenchuan earthquake using a Bayesian technique. Eng. Geol. 280, 105965.
- Johnson, K.A., Sitar, N., 1990. Hydrologic conditions leading to debris-flow initiation. Can. Geotech. J. 27, 789–801.
- Ju, N., Huang, J., He, C., Van Asch, T.W.J., Huang, R., Fan, X., Xu, Q., Xiao, Y., Wang, J., 2020. Landslide early warning, case studies from Southwest China. Eng. Geol. 279, 105917.
- Kirschbaum, D., Stanley, T., 2018. Satellite-based assessment of rainfall-triggered landslide hazard for situational awareness. Earth's Future 6, 505–523.
- Krajewski, W.F., Ciach, G.J., Habib, E., 2003. An analysis of smallscale rainfall variability in different climatic regimes. Hydrol. Sci. J. 48, 151–162.

Li, J., Liu, Z., Wang, R., Zhang, X., Liu, X., Yao, Z., 2022. Analysis of debris flow triggering conditions for different rainfall patterns based on satellite rainfall products in Hengduan Mountain region, China. Remote Sens. 14, 2731.

- Lu, C., Ye, J., Fang, G., Huang, X., Yan, M., 2021. Assessment of GPM IMERG satellite precipitation estimation under complex climatic and topographic conditions. Atmosphere 12 (6), 780.
- Ma, H., Zeng, J., Chen, N., Zhang, X., Cosh, M.H., Wang, W., 2019. Satellite surface soil moisture from SMAP, SMOS, AMSR2 and ESA CCI: a comprehensive assessment using global ground-based observations. Remote Sens. Environ. 231, 111215.
- Marino, P., Peres, D.J., Cancelliere, A., Greco, R., Bogaard, T.A., 2020. Soil moisture information can improve shallow landslide forecasting using the hydrometeorological threshold approach. Landslides 17, 2041–2054.
- Mathew, J., Babu, D.G., Kundu, S., Kumar, K.V., Pant, C.C., 2014. Integrating intensity-duration-based rainfall threshold and antecedent rainfall-based probability estimate towards generating early warning for rainfall-induced landslides in parts of the Garhwal Himalaya, India. Landslides 11, 575–588.
- Mirus, B.B., Morphew, M.D., Smith, J.B., 2018. Developing hydro-meteorological thresholds for shallow landslide initiation and early warning. Water 10 (9), 1274.
- Neptune, C.K., Degraff, J.V., Pluhar, C.J., Lancaster, J.T., Staley, D.M., 2021. Rainfall thresholds for post-fire debris-flow generation, Western Sierra Nevada, CA. Environ. Eng. Geosci. 27 (4), 439–453.
- Ni, H., Song, Z., 2020. Response of debris flow occurrence to daily rainfall pattern and critical rainfall condition in the Anning River-Zemu River Fault Zone, SW China. B Eng. Geol. Environ. 79, 1735–1747.
- Nikolopoulos, E.I., Crema, S., Marchi, L., Marra, F., Guzzetti, F., Borga, M., 2014. Impact of uncertainty in rainfall estimation on the identification of rainfall thresholds for debris flow occurrence. Geomorphology 221, 286–297.
- Nikolopoulos, E.I., Destro, E., Maggioni, V., Marra, F., Borga, M., 2017. Satellite rainfall estimates for debris flow prediction: an evaluation based on rainfall accumulationduration thresholds. J. Hydrometeorol. 18, 2207–2214.
- Peres, D.J., Cancelliere, A., Greco, R., Bogaard, T.A., 2018. Influence of uncertain identification of triggering rainfall on the assessment of landslide early warning thresholds. Nat. Hazards Earth Syst. Sci. 18, 633–646.
- Pradhan, R.K., Markonis, Y., Vargas Godoy, M.R., Villalba-Pradas, A., Andreadis, K.M., Nikolopoulos, E.I., Papalexiou, S.M., Rahim, A., Tapiador, F.J., Hanel, M., 2022. Review of GPM IMERG performance: a global perspective. Remote Sens. Environ. 268, 112754.
- Ray, R., Jacobs, J., Cosh, M.H., 2010. Landslide susceptibility mapping using downscaled AMSR-E soil moisture: a case study from Cleveland Corral, California, US. Remote Sens. Environ. 114, 2624–2636.
- Sahlu, D., Nikolopoulos, E.I., Moges, S.A., Anagnostou, E.N., Hailu, D., 2016. First evaluation of the Day-1 IMERG over the Upper Blue Nile Basin. J. Hydrometeorol. 17 (11), 2875–2882.
- Sakib, S., Ghebreyesus, D., Sharif, H.O., 2021. Performance evaluation of IMERG GPM products during Tropical Storm Imelda. Atmosphere 12 (6), 687.
- Salles, L., Satgé, F., Roig, H., Almeida, T., Olivetti, D., Ferreira, W., 2019. Seasonal effect on spatial and temporal consistency of the new GPM-based IMERG-v5 and GSMaP-v7 satellite precipitation estimates in Brazil's central plateau region. Water 11 (4), 668.
- Simoni, S., Bernard, M., Boreggio, M., Lanzoni, S., Stancanelli, L.M., Berti, M., Gregoretti, C., 2020. Runoff-generated debris flows: Observation of initiation conditions and erosion-deposition dynamics along the channel at Cancia (eastern Italian Alps). Earth Surf. Process. Landf. 45, 3556–3571.
- Siuki, S.K., Saghafian, B., Moazami, S., 2017. Comprehensive evaluation of 3-hourly TRMM and half-hourly GPM-IMERG satellite precipitation products. Int. J. Remote Sens. 38 (2), 558–571.
- Staley, D.M., Kean, J.W., Cannon, S.H., Schmidt, K.M., Laber, J.L., 2013. Objective definition of rainfall intensity-duration thresholds for the initiation of post-fire debris flows in southern California. Landslides 10, 547–562.
- Tan, J., Petersen, W.A., Kirstetter, P.-E., Tian, Y., 2017. Performance of IMERG as a function of spatiotemporal scale. J. Hydrometeorol. 18 (2), 307–319.
- Tang, G., Clark, M.P., Papalexiou, S.M., Ma, Z., Hong, Y., 2020. Have satellite precipitation products improved over last two decades? A comprehensive comparison of GPM IMERG with nine satellite and reanalysis datasets. Remote Sens. Environ. 240, 111697.
- Thakur, M.K., Kumar, T.V.L., Rao, K.K., Barbosa, H., Rao, V.B., 2019. A new perspective in understanding rainfall from satellites over a complex topographic region of India. Sci. Rep. 9, 15610.
- Thakur, M.K., Kumar, T.V.L., Narayanan, M.S., Kundeti, K.R., Barbosa, H., 2020. Analytical study of the performance of the IMERG over the Indian landmass. Meteorol. Appl. 27, e1908.
- Tien Bui, D., Pradhan, B., Lofman, O., Revhaug, I., Dick, Ø.B., 2013. Regional prediction of landslide hazard using probability analysis of intense rainfall in the Hoa Binh province, Vietnam. Nat. Hazards 66 (2), 707–730.
- Tsai, T.-L., Chen, H.-F., 2010. Effects of degree of saturation on shallow landslides triggered by rainfall. Environ. Earth Sci. 59, 1285–1295.
- Uwihirwe, J., Riveros, A., Wanjala, H., Schellekens, J., Weiland, F.S., Hrachowitz, M., Bogaard, T.A., 2022. Potential of satellite-derived hydro-meteorological information for landslide initiation thresholds in Rwanda. Nat. Hazards Earth Syst. Sci. 22, 3641–3661.
- Vasu, N.N., Lee, S., Pradhan, A.M.S., Kim, Y., Kang, S., Lee, D., 2014. A new approach to temporal modelling for landslide hazard assessment using an extreme rainfall induced-landslide index. Eng. Geol. 215, 36–49.
- Wagner, W., Lemoine, G., Rott, H., 1999. A method for estimating soil moisture from ERS Scatterometer and soil data. Remote Sens. Environ. 70, 191–207.

- Wang, Y., Leng, P., Peng, J., Marzahn, P., Ludwig, R., 2021a. Global assessments of two blended microwave soil moisture products CCI and SMOPS with in-situ measurements and reanalysis data. Int. J. Appl. Earth Obs. 94, 102234.
- Wang, N., Lombardo, L., Gariano, S.L., Cheng, W., Liu, C., Xiong, J., Wang, R., 2021b. Using satellite rainfall products to assess the triggering conditions for hydromorphological processes in different geomorphological settings in China. Int. J. Appl. Earth Obs. 102, 102350.
- Wicki, A., Lehmann, P., Hauck, C., Seneviratne, S.I., Waldner, P., Stähli, M., 2020. Assessing the potential of soil moisture measurements for regional landslide early warning. Landslides 17, 1881–1896.
- Yang, H., Wei, F., Ma, Z., Guo, H., Su, P., Zhang, S., 2020. Rainfall threshold for landslide activity in Dazhou, southwest China. Landslides 17 (1), 61–77.
- Yang, H., Zhang, S., Hu, K., Wei, F., Wang, K., Liu, S., 2022. Field observation of debrisflow activities in the initiation area of the Jiangjia Gully, Yunnan Province, China. J. Mt. Sci. Engl. 19 (6), 1602–1617.
- Yu, C., Hu, D., Di, Y., Wang, Y., 2021. Performance evaluation of IMERG precipitation products during typhoon Lekima (2019). J. Hydrol. 597, 126307.
- Zhou, W., Tang, C., 2014. Rainfall thresholds for debris flow initiation in the Wenchuan earthquake-stricken area, southwestern China. Landslides 11, 877–887.
- Zhou, C., Gao, W., Hu, J., Du, L., Du, L., 2021. Remote Sens. 13 (4), 689.
- Zhuang, J., Cui, P., Wang, G., Chen, X., Iqbal, J., Guo, X., 2015. Rainfall thresholds for the occurrence of debris flows in the Jiangjia Gully, Yunnan Province, China. Eng. Geol. 195, 335–346.
- Zhuo, L., Dai, Q., Han, D., Chen, N., Zhao, B., Berti, M., 2019. Evaluation of remotely sensed soil moisture for landslide hazard assessment. IEEE J. Sel. Topics Appl. Earth Observ. Remote Sens. 12 (1), 162–173.